The Interannual Variability of East Asian Monsoon and Its Relationship with SST in a Coupled Atmosphere–Ocean–Land Climate Model

Wang Huijun (王会军)①

Laboratory for Numerical Modeling of Atmospheric Science and Geophysical Fluid Dynamics (LASG),
Institute of Atmospheric Physics, Chinese Academy of Sciences, Beijing 100029

(Received April 29, 1999; revised July 2, 1999)

ABSTRACT

Based on a 200 year simulation and reanalysis data (1980–1996), the general characteristics of East Asian monsoon (EAM) were analyzed in the first part of the paper. It is clear from this research that the South Asian monsoon (SAM) defined by Webster and Yang (1992) is geographically and dynamically different from the East Asian monsoon (EAM). The region of the monsoon defined by Webster and Yang (1992) is located in the tropical region of Asia (40–110°E, 10–20°N), including the Indian monsoon and the Southeast Asian monsoon, while the EAM defined in this paper is located in the subtropical region of East Asia (110–125°E, 20–40°N). The components and the seasonal variations of the SAM and EAM are different and they characterize the tropical and subtropical Asian monsoon systems respectively. A suitable index (EAMI) for East Asian monsoon was then defined to describe the strength of EAM in this paper.

In the second part of the paper, the interannual variability of EAM and its relationship with sea surface temperature (SST) in the 200 year simulation were studied by using the composite method, wavelet transformation, and the moving correlation coefficient method. The summer EAMI is negatively correlated with ENSO (El Nino and Southern Oscillation) cycle represented by the NINO3 sea surface temperature anomaly (SSTA) in the preceding April and January, while the winter EAM is closely correlated with the succeeding spring SST over the Pacific in the coupled model. The general differences of EAM between El Nino and La Nina cases were studied in the model through composite analysis. It was also revealed that the dominating time scales of EAM variability may change in the long-term variation and the strength may also change. The anomalous winter EAM may have some correlation with the succeeding summer EAM, but this relationship may disappear sometimes in the long-term climate variation. Such time-dependence was found in the relationship between EAM and SST in the long-term climate simulation as well.

Key words: East Asian monsoon, Interannual variability, Coupled climate model

1. Introduction

The largest interannual variability associated with the ENSO cycle exists in monsoon regions like the African monsoon, Australian monsoon, Pan-American monsoon and Asian monsoon (Ropelewski and Halpert, 1987; Webster and Yang, 1992; Ju and Slingo, 1995). One basic question is how to represent the Asian monsoon and its variability. Webster and Yang (1992) found a reasonable index by averaging the zonal wind shear between 850 hPa and 200

①Fax 86-10-62028604; E-mail wanghj@lasgsgi4.iap.ac.cn

hPa over the South Asian region (40–110°E, 0°–20°N) to describe the South Asian monsoon circulation and its variability. Recently, Gaswami et al. (1997) defined the extended Indian monsoon rainfall index and the monsoon Hadley circulation index (the meridinal wind shear between 850 hPa and 200 hPa) over the region (70–110°E, 10–30°N) to describe the strength of the South Asian monsoon. In contrast to these two definitions, Wang and Fan (1998) suggested using the zonal wind shear index or the OLR (outgoing long-wave radiation) index computed over the Indian monsoon region and the Southeast Asian monsoon region to describe the two monsoon systems separately. They argued that interannual variations of the wind shear in the two regions are weakly correlated hence it is more appropriate to describe the two monsoon systems separately.

While the Webster and Yang index is suitable for representing the large scale tropical monsoon circulation in Asia and its relationship with the ENSO cycle, such an index is not well suited to describing the East Asian monsoon (EAM). The domain of the EAM includes the eastern part of China, the Korean peninsula and South Japan, with the major area bounded by 110–125°E, 20–40°N. Meanwhile the domain of the South Asian monsoon defined by Webster and Yang (1992) is 40–110°E, 0°–20°N, covering India, and the Indo-China peninsula. Hence, the two monsoon systems are located in the tropics and sub-tropics respectively and they have different features from an atmospheric circulation point of view (Fig. 1).

As reviewed by Tao and Chen (1987), the major components of the EAM circulation are the western Pacific subtropical high, the cross-equatorial flow in the lower atmosphere over the South China Sea, the monsoon trough and the Meiyu front. Meanwhile the SAM consists mainly of the Mascarene high, the Somali jet and the westerly wind in the region.

The seasonal variation characteristics of the EAM and the SAM are different. The SAM is characterized by monsoon onset, monsoon breaks, and monsoon closing. In the EAM region the monsoon rain-belt moves northward from spring to summer and retreats southward in late summer and autumn.

The model used in this study is the coupled atmosphere–ocean–land climate model developed at the Laboratory of Numerical Modeling for Atmospheric Science and Geo-

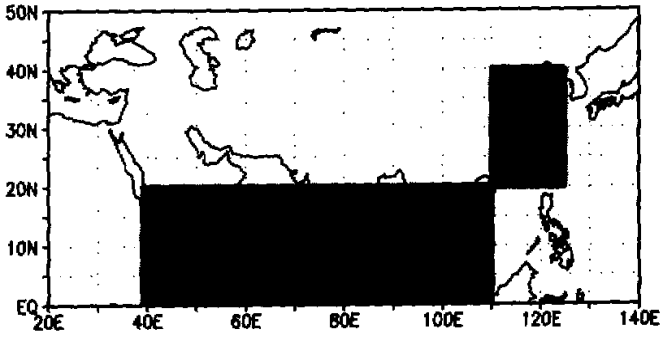

Fig. 1. The geographical locations of 'Asian monsoon' defined by Webster and Yang (1992) and EAM defined in this paper.

physical Fluid Dynamics (LASG) at the Institute of Atmospheric Physics (IAP). The NCEP / NCAR (National Center for Environmental Prediction / National Center for Atmospheric Research) monthly reanalysis data was used for the validation of the model results. The long term variability of the EAM and its relationship with SST in the 200 year run were also analyzed.

2. The model and the methodology of analysis

The atmospheric part of the coupled model is a R15L9 model developed from Simmonds (1985) (Wu et al., 1996). The ocean part is the Institute of Atmospheric Physics $4^\circ \times 5^\circ$L20 free surface oceanic general circulation model (Zhang et al., 1996). Both the atmospheric and oceanic models adopted the so called standard atmosphere subtraction scheme developed by Zeng et al. (1989) to reduce the large truncation errors in the high topography regions. The land surface process model is the modified simple biosphere model developed by Sellers et al. (1986) and by Xue et al. (1991). The coupling of the models and the integration were completed by Yu (1998) and the monthly mean of model output was re-organized by Yu for the convenient use of the climate community in the IAP. Preliminary analysis showed ENSO like variability in the 200 year integration and there is very small climate drift (Yu, 1997; Wu et al., 1997).

The NCEP / NCAR reanalysis monthly data (1980–1996) were used for comparison with the model results.

The moving correlation coefficient method, alongside wavelet analysis, composite analysis, and the correlation coefficient method, is used in this paper. The method is as follows:

Let $X(i)$ and $Y(i)$($i = 1,2,\cdots,N$) be the 2 time series and $X'(j)$ and $Y'(j)$($j = 1,2,\cdots,N,\cdots N + 30$) be the extended time series of $X(i)$ and $Y(i)$ respectively. Then we compute the correlation coefficient $R(i)$ on every i point between $X(i)$ and $Y(i)$. When computing $R(i)$, we use 31 samples of $X'(j)$ and $Y'(j)$($j = i,i+1,\cdots,i+30$) in which $X'(j)$ and $Y'(j)$ are comprised as follows:

$$X(i): X(15),X(14),\cdots,X(3),X(2),X(1),X(2),\cdots,X(i),\cdots,X(N),X(N-1),X(N-2),\cdots,X(N-15)$$

$$X'(j): X'(1),X'(2),\cdots,X'(14),X'(15),X'(16),X'(17),\cdots,X'(i+15),\cdots,X'(N+15),X'(N+16),X'(N+17),\cdots,X'(N+30)$$

$$Y(i): Y(15),Y(14),\cdots,Y(3),Y(2),Y(1),Y(2),\cdots,Y(i),\cdots,Y(N),Y(N-1),Y(N-2),\cdots,Y(N-15)$$

$$Y'(j): Y'(1),Y'(2),\cdots,Y'(14),Y'(15),Y'(16),Y'(17),\cdots,Y'(i+15),\cdots,Y'(N+15),Y'(N+16),Y'(N+17),\cdots,Y'(N+30)$$

This method is used in studying the change of the correlation between two time series in a long-term variation.

3. The general characteristics of EAM and the EAM index

The most striking feature besides the seasonal movement of the EAM rain-belt over eastern China is the summer north wind component, which has the same magnitude as the zonal wind component, along the western edge of the subtropical high over the western Pacific in the low level atmosphere. Comparatively, the north wind component of SAM is much smaller than the zonal wind component in the low level atmosphere. These two monsoon wind systems at 850 hPa are well simulated by the LASG coupled model as shown in Fig. 2. The model results agree quantitatively well with the NCEP / NCAR reanalysis.

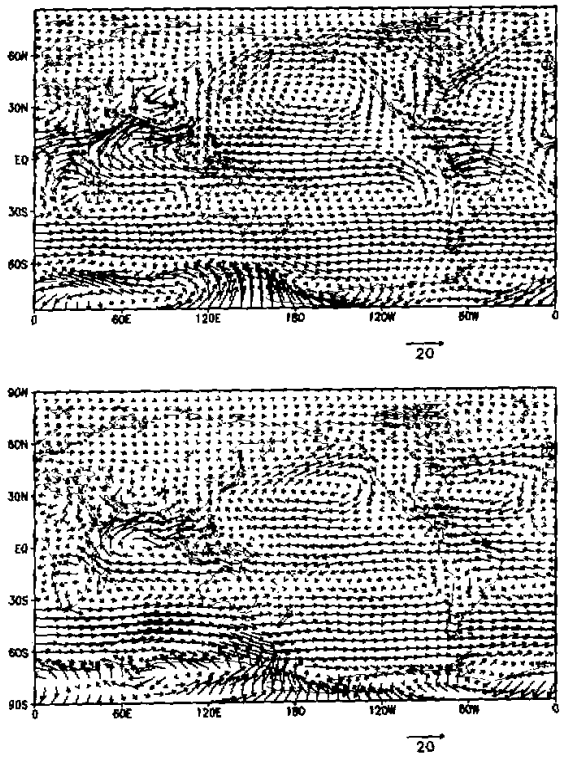

Fig. 2. The global distributions of JJA wind velocity (m / s) climatology at 850 hPa in LASG coupled model (a); and NCEP / NCAR reanalysis (1980–1996) (b).

Based on the above considerations, we define an EAM index EAMI as follows:

$$I_{\mathrm{EAM}} = (u' + v') / 2^{1/2},$$

averaged over (110–125°E, 20–40°N) as denoted in Fig. 1. Here u' and v' are the zonal and meridional wind departures from the zonal average at 850 hPa respectively.

As noted by Tao and Chen (1987) when the EAM is stronger the summer precipitation anomaly is negative over the Huaihe River valley and the Yangtze River valley and positive over central North China. We do find similar relationships in the model simulation. The correlation between EAMI and precipitation for JJA(June–July–August) is positive over North China, the Korea Peninsula and part of Japan and negative in the Yangtze River valley (Fig. 3). This illustrates that EAMI could represent the strength of the EAM and the pattern of precipiation anomaly related with the EAM. EAMI could represent the contrast of land–sea pressure and the close link between EAM and the subtropical high over the western Pacific as well as in the NCEP / NCAR reanalysis shown in Figs. 4 and 5. EAMI is positively correlated with sea–level pressure over the western Pacific and negatively over the East Asian continent. The pattern of the correlation between EAMI and geopotential height at 500 hPa is similar to that of EAMI and sea–level pressure correlation. EAMI can represent the low level atmospheric thermal contrast between the East Asian continent and the western Pacific

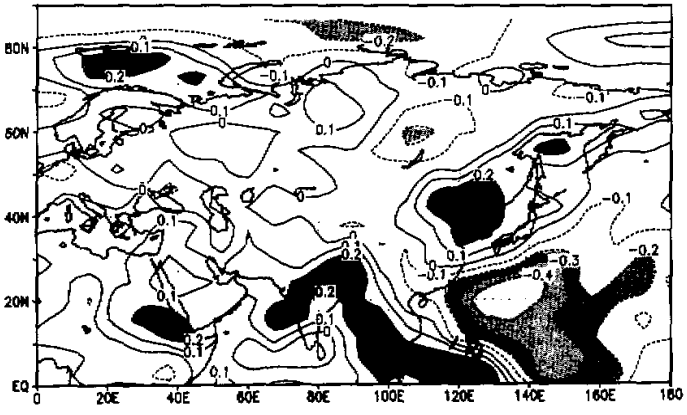

Fig. 3. The distribution of the correlation between EAMI and precipitation during JJA in LASG coupled model. Area with statistical significance at 95% level were shaded.

as well (figure not shown).

EAMI is negatively correlated with the zonal wind at 850 hPa over a large part of the SAM region (from 80°E to 110°E) and over part of the western Pacific (110–160°E) between 0°–20°N both in the NCEP / NCAR reanalysis and the coupled model as shown in Fig. 6. It is interesting also to note that EAMI is correlated with JJA rainfall over India and the Indo–China Peninsula in the LASG coupled model simulation (Fig. 3). Thus there is some relationship between EAM and SAM but basically they are geographically and dynamically different.

4. The interannual variability of summer EAM

The 200 year simulation suggests that JJA EAMI is negatively correlated with NINO3 SSTA in the preceding January and April (correlation coefficients are −0.23 and −0.21 respectively). These correlations are statistically significant at the 95% level. But the simultaneous correlation is comparatively weak. There is also significant correlation between JJA EAMI and NINO3 SSTA during the succeeding December at −0.15. The temporal variation of JJA EAMI and NINO3 SSTA in January is plotted in Fig. 7.

We also carried out a composite analysis on the 200 year simulation to get further insight on the relationship between the East Asian monsoon and the ENSO cycle. There are 50 years in which the NINO3 SSTA in April is larger than 0.20°C and 55 years with NINO3 SSTA less than −0.20°C. Thus we compare the 50 years composite as the ' El Nino' case with the 55 years composite as the ' La Nina' case.

The difference of JJA velocity at 850 hPa between the ' El Nino' case and the ' La Nina' case is plotted in Fig. 8. We can easily find the northeast wind anomaly over the EAM region and the westerly wind anomaly over a large part of the SAM region and tropical western Pacific. This again supports the negative relationship between summer EAM and NINO3 SSTA

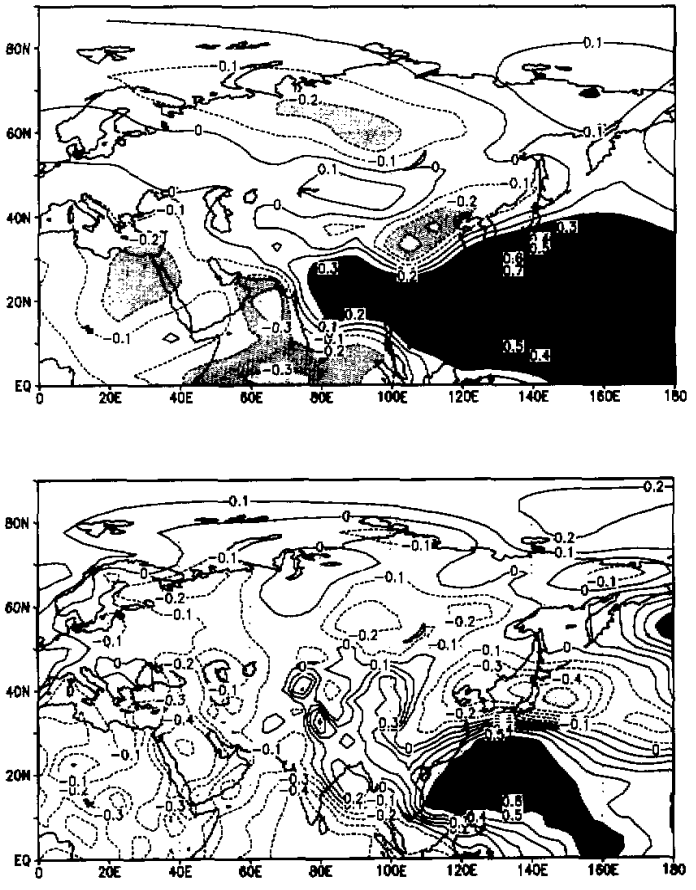

Fig. 4. The distribution of the correlation between EAMI and sea-level pressure during JJA in LASG coupled model (a); and NCEP / NCAR reanalysis (1980–1996) (b). Areas with statistical significance at 95% level were shaded.

in the preceding months. It also shows clearly that the EAM and SAM are different monsoon systems in wind field.

In the ' El Nino' case, the ocean–land contrast in sea-level pressure for EAM is weaker than that in the ' La Nina' case, with a positive sea-level pressure difference over the northern Asian continent but a negative difference over the western Pacific ocean (Fig. 9). At the 10 hPa level the JJA air temperature is significantly higher in the ' El Nino' case than in the ' La Nina' case over a large area of Asia as shown in Fig. 10.

Large area including most parts of India, Tibet and the western part of the Indo-China Peninsula is covered with negative JJA precipitation difference between ' El Nino' and ' La Nina' composites. Negative JJA precipitation difference is also located over South China and

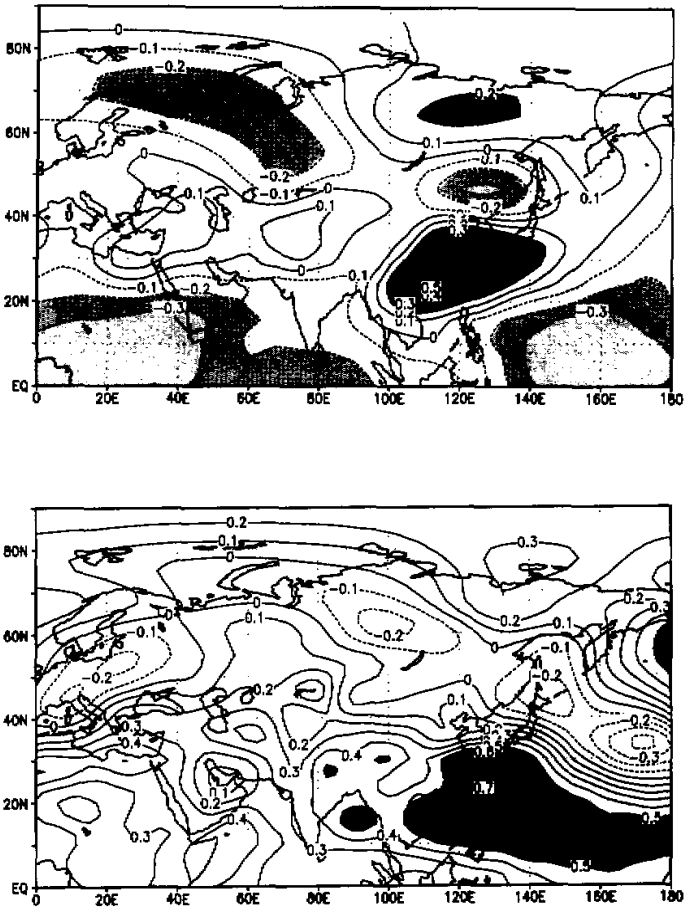

Fig. 5. Same as Fig. 4, but for the correlation of EAMI and 500 hPa geopotential height.

part of the Yellow River valley, while positive difference exists over the Huaihe River valley. But, these differences are mostly insignificant at the 95% significance level (Fig. 11). Thus the coupled model does not show strong correlation between NINO3 SST and JJA precipitation over East Asia.

In order to study the long-term variation of the EAM, we carried out a wavelet transformation on EAMI and NINO3 SSTA. From Fig. 12, it is clear that there are multi-scales in the temporal evolution and that the dominant time scales and their strength may change from one period to another. For example, in the first 40 years the main scales of variation are 1–2 years scale and 10–20 years scale, meaning that interannual and decadal scale variability are both significant. There is also 80–100 years scale of variation during this period. While in the last 100 years of the simulation, the decadal scale variation is weaker and there is almost

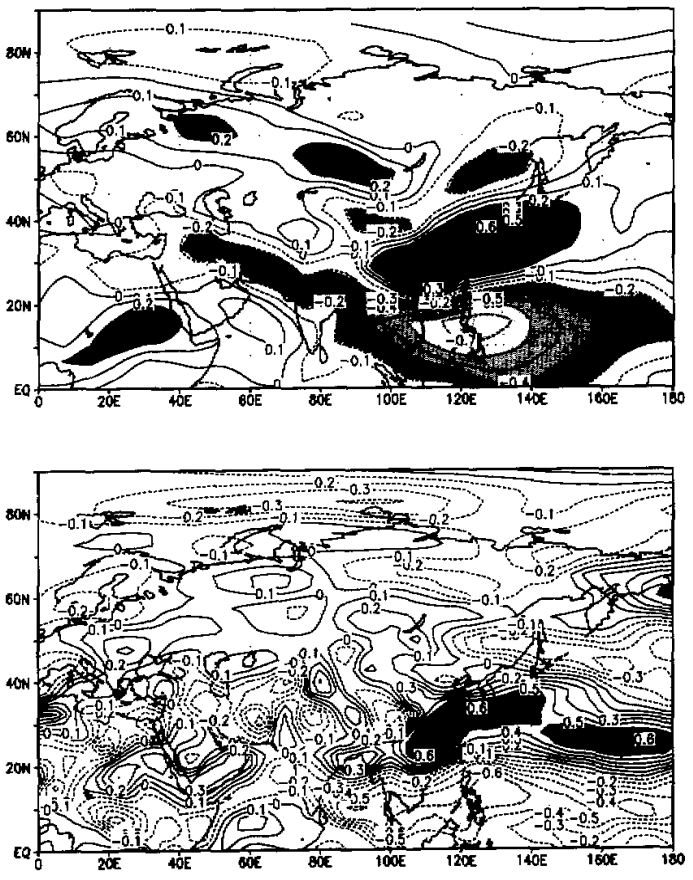

Fig. 6. Same as Fig. 4, but for the correlation of EAMI and 850 hPa zonal wind.

no centennial scale variation. In addition, during this period the interannual signal is stronger compared to the first 40 year period.

We also find such multi-scale variability in the NINO3 SSTA. It is interesting to note that the correlation between JJA EAMI and NINO3 SSTA is different in different time scales in Table 1. In the long time scales (larger than 8 years) the correlation of JJA EAMI to NINO3 SSTA in any month is always negative. While in the short time scales (2 years and 4 years), the correlation is variable with month and generally weaker compared to the long term correlation. Over the 2 year time scale, JJA EAMI is negatively correlated with preceding January NINO3 SSTA and positively correlated with succeeding December NINO3 SSTA. Over the 4 year time scale, JJA EAMI is negatively correlated with preceding January or April NINO3 SSTA and positively correlated with succeeding October NINO3 SSTA. All the correlations mentioned above are statistically significant at the 95% level and the various time scales of variation were studied by means of wavelet (using Morlet function) transformation.

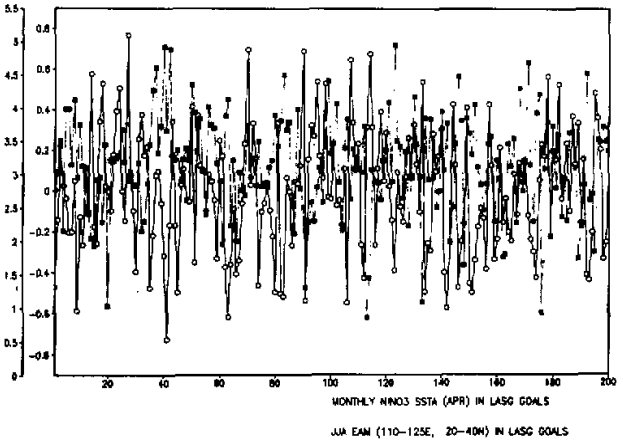

Fig. 7. The interannual variation of EAMI (m / s) during JJA and NINO3 SSTA (°C) during January in the coupled model. ○ for NINO3 SSTA and ■ for EAMI.

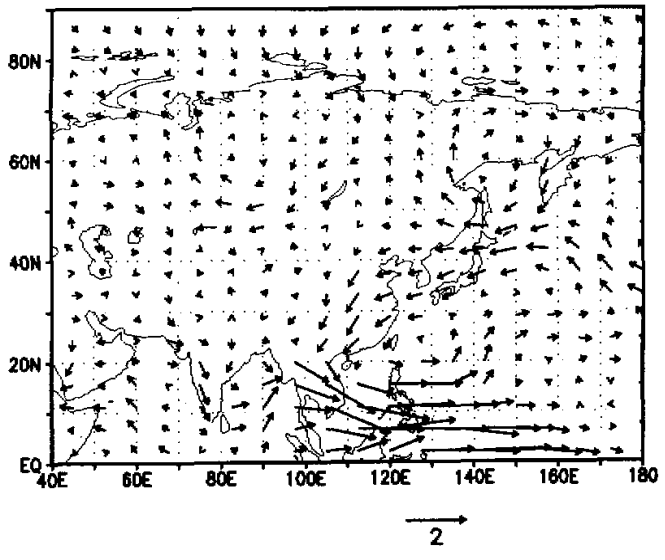

Fig. 8. The geographical distribution of JJA wind velocity difference (m / s) at 850 hPa between El Nino and La Nina composites in the coupled model defined by NINO3 SSTA at April larger than 0.20°C or lower than −0.20°C respectively. Areas with statistical significance at 95% level were shaded.

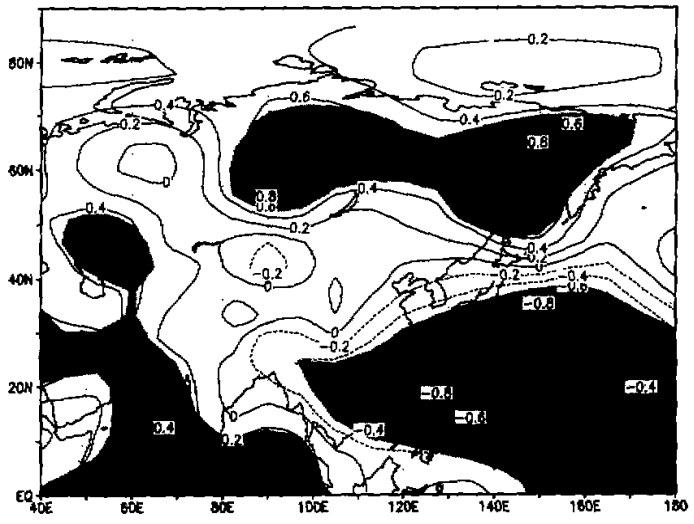

Fig. 9. Same as Fig. 8, but for sea-level pressure difference (hPa). Areas with statistical significance at 95% level were shaded.

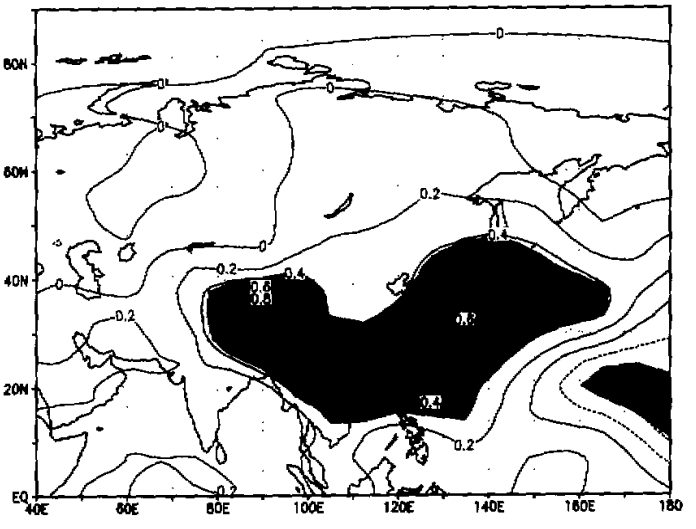

Fig. 10. Same as Fig. 9, but for the air temperature difference at 10 hPa (°C).

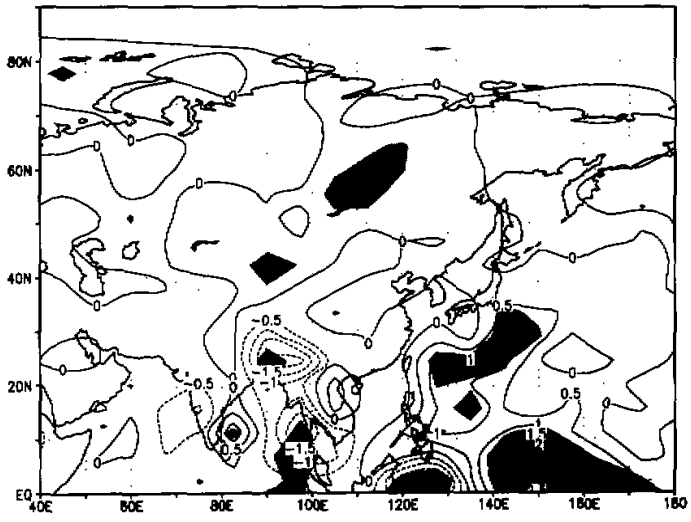

Fig. 11. Same as Fig. 9, but for precipitation difference (mm / d).

Table 1. Correlations between JJA EAMI and NINO3 SSTA in different months and annual mean. The correlation is changed with time scales (2 year, 4 year, and so on) in wavelet transformation (using Morlet function) as simulated by the LASG coupled model (200 years simulation). In the table 'Annual' stands for correlation of annual mean SSTA and JJA EAMI in different time scales, and 'Jan. Apr. Jul. Oct. Dec.' stand for January, April, July, October, and December respectively

	2 yr	4 yr	8 yr	16 yr	32 yr	64 yr	128 yr
Annual	−0.06	−0.00	−0.44	−0.42	−0.85	−0.52	−0.84
Jan.	−0.24	−0.13	−0.28	−0.47	−0.85	−0.08	−0.87
Apr.	−0.07	−0.16	−0.11	−0.24	−0.79	0.12	−0.86
Jul.	−0.04	0.00	−0.17	−0.27	−0.53	−0.76	−0.73
Oct.	0.03	0.21	−0.44	−0.19	−0.67	−0.67	−0.51
Dec.	0.23	−0.10	−0.40	−0.27	−0.82	−0.55	−0.81

5. The interannual variability of winter EAM

As noted by Li (1988), strong cold surge activities in East Asia may play an important role in the El Nino occurrence. Since the instrumental record is too short to get a statistical conclusion on this relationship, it is a reasonable way to study the long-term integration of the comprehensive coupled climate model. We did find such a relationship in the LASG coupled model run. The average meridional wind departure from the zonal mean in the EAM region during January and February was used as the winter EAM index. The correlation

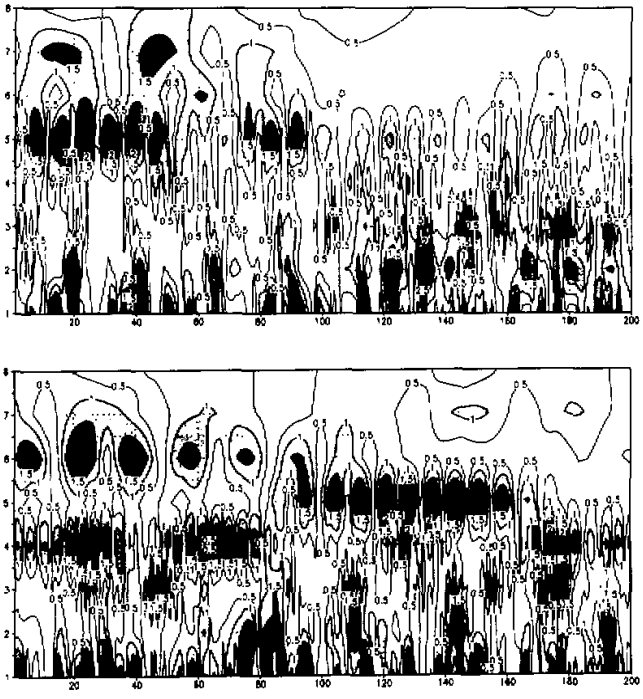

Fig. 12. The wavelet transformations (using Morlet function) for JJA EAMI (a); and January NINO3 SSTA (b). The EAMI and NINO3 SSTA were normalized before the transformation. The abscissa is time in year and the ordinate is $a(2^{a-1}$ is the time scale in Morlet function).

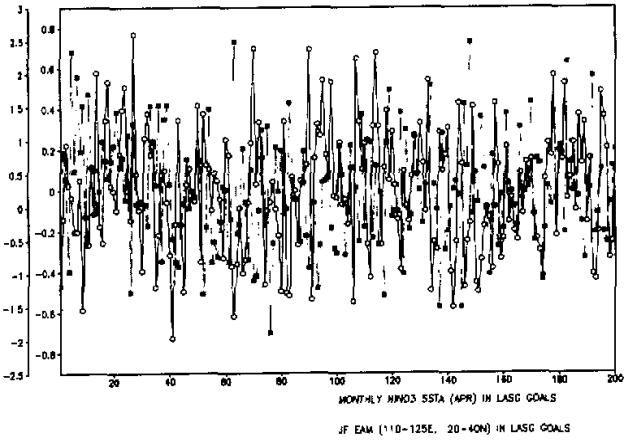

Fig. 13. Same as Fig. 7, but for winter EAM index and NINO3 SSTA in May.

coefficients between the winter EAM index and the NINO3 SSTA in March, April, and May are −0.17, −0.19, and −0.18 respectively. While the simultaneous correlation coefficients are only −0.12 and −0.18 in January and February respectively. The interannual variation of the winter EAM index and NINO3 SSTA in May is plotted in Fig. 13.

As could be seen from Fig. 14, the winter EAM index is correlated with SSTA positively in the Kuroshio region and negatively in the central and eastern tropical Pacific during January through June. We note that the above correlation is strongest in the Kuroshio region and central tropical Pacific around the date line, and relatively weaker in the eastern tropical Pacific (Fig. 14).

The winter EAM is to some extent an indication of the large-scale general circulation over Eurasia and Pacific, as may be seen through composite analysis shown in Fig. 15. The EUP (Eurasia–Pacific) teleconnection pattern is very clear in the correlation between the winter EAM index with 500 hPa geopotential height or with 1000 hPa air temperature in January. The correlation coefficient between winter EAM index and EUP index is −0.52,

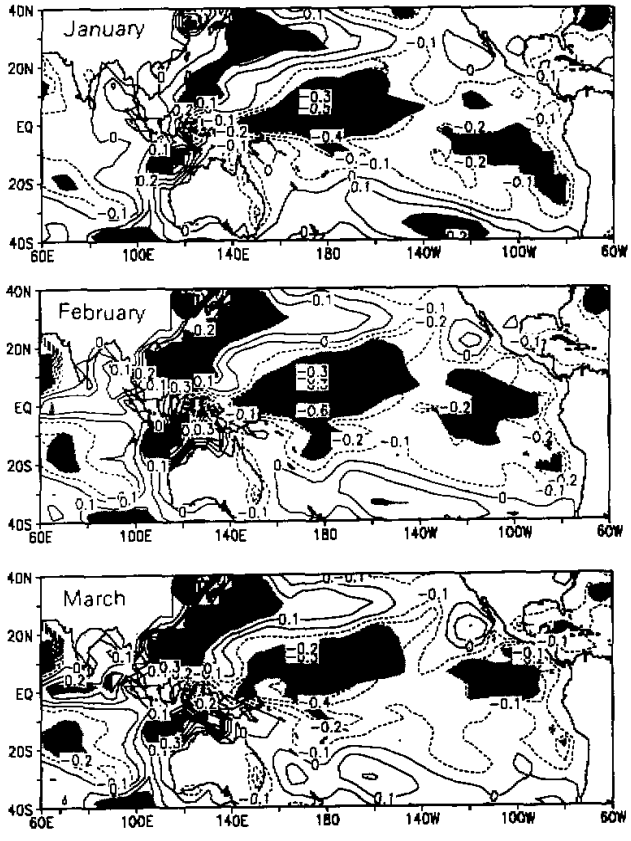

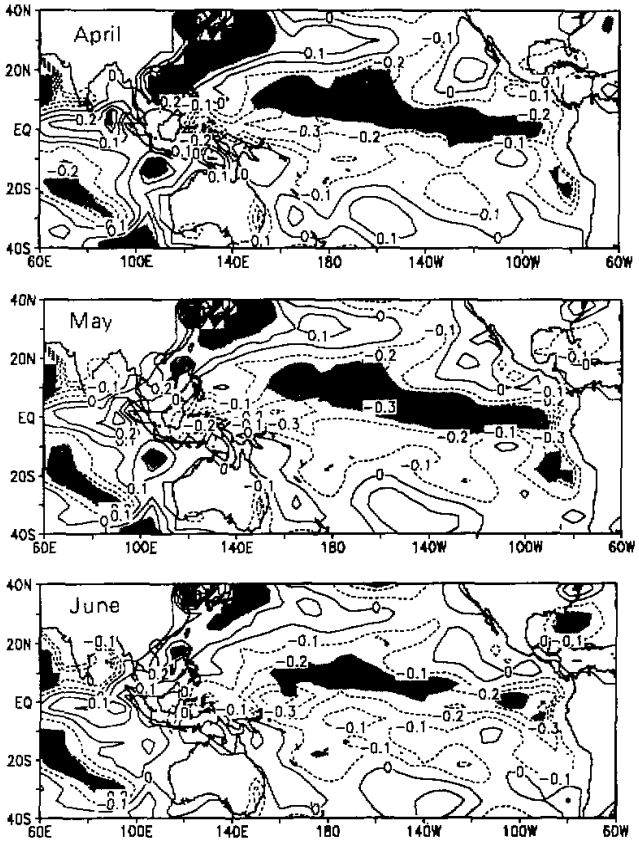

Fig. 14. The geographical distribution of the correlation coefficient between winter EAM index and SSTA in January, February, March, April, May and June.

indicating the close interrelation of the EUP pattern and winter EAM. However, the winter EAM index is more correlated to NINO3 SSTA than EUP index in the model. Therefore, it is more likely that the EUP anomaly pattern may play an indirect role in the occurrence of an El Nino.

6. Concluding remarks

From the above studies, we may conclude that EAM as a subtropical monsoon system is geographically and dynamically different from the tropical monsoon system SAM. Evidence from the NCEP/NCAR reanalysis and the long term integration of the LASG coupled model suggest that mean southwest wind departure from the zonal average at 850 hPa over (110–125°E, 20–40°N) is a good index for the study of summer EAM circulation and its interannual variation. EAMI is related with all the major features of EAM, such as the land–ocean sea–level pressure contrast, the close link of EAM with the subtropical high

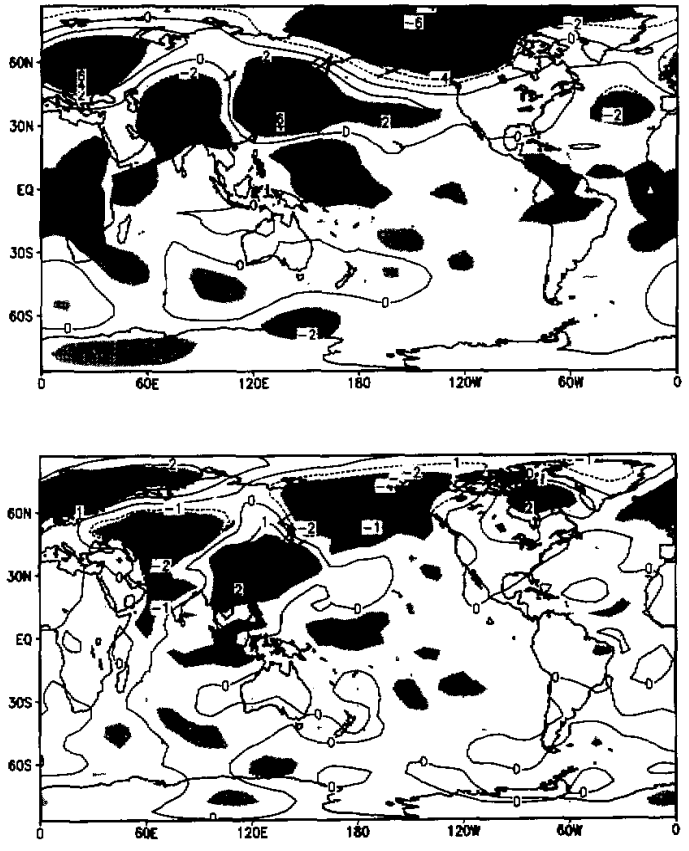

Fig. 15. The geographical distributions of differences in 500 hPa geopotential height in m (a); and 1000 hPa air temperature in °C (b) for January between weak and strong winter EAM composites in LASG coupled model simulation.

over the western Pacific, the relationship of EAM and the summer rainfall over East China and the negative correlation of EAM and SAM wind fields. While the mean meridional wind in the same region during winter can be used as the winter EAM index.

The summer EAMI is negatively correlated with preceding NINO3 SSTA in January or April and succeeding NINO3 SSTA in December (−0.23, −0.21 and −0.15 respectively) in the LASG coupled model. But the correlation is variable in the different time scale components through wavelet transformation analysis. In the time scales larger than the decadal scale the JJA EAMI is always negatively correlated with NINO3 SSTA in any month. While in the interannual time scales the correlation is changeable depending on the month in which the NINO3 SSTA is concerned.

In different periods, the dominant time scales of variation are different for EAMI and NINO3 SSTA in LASG coupled model. This result agrees with the long term reconstructed

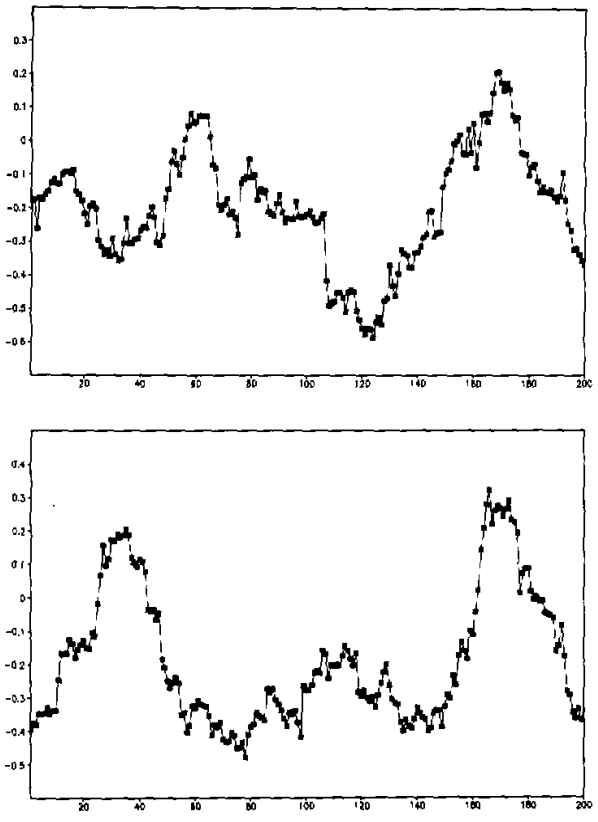

Fig. 16. The moving correlation coefficient between JJA EAMI and NINO3 SSTA in preceding April (a); and between winter EAM index and NJNO3 SSTA in succeeding April (b).

paleo–SST data (Cole, 1998)①.

The meridional wind component departure from the zonal mean at 850 hPa during January and February is used as the winter EAM index in this paper. One major finding through analyzing the long–term integration of the LASG coupled model is that the winter EAM index is correlated with SST in the succeeding spring, supporting results noted previously (Li, 1988). It is found also that the interannual variation of winter EAM can represent the interannual variation of the EUP (Europe–Pacific) teleconnection pattern to some extent. Therefore, it seems that there is an indirect relationship between winter the EUP pattern and the SSTA in the succeeding spring. It is interesting to note that winter EAM is correlated with the succeeding summer EAM during some periods (e.g., year 81–111 period).

It is revealed that the lag correlation between the SSTA and the EAM may vary in a long–term climate variation. By using the moving correlation coefficient method, we found

①personal communication

the correlation coefficient between JJA EAMI and NINO3 SSTA in the succeeding April to be −0.51 (close correlation) during the period 111−141 yr and −0.1 (very weak correlation) during the period 151−181 yr. It seems that weak correlation is linked with low ENSO variance. This result agrees with the finding in the last hundred years of observation in which there is no relation between the Asian monsoon and ENSO between 1920−1960 (Ju and Slingo, 1995; National Research Council, 1996). We also found such a time−dependence of the correlation between winter EAM and SSTA (Fig. 16).

The author wishes to thank Profs. Wu G.X., Zhang X.H., and Dr. Yu Y.Q. for providing the coupled model results. Dr. Yu also kindly provided assistance in using the model output. This work was supported jointly by the National Natural Science Foundation of China key project "The analysis on the seasonal−to−interannual variation of the general circulation" under contract 49735160 and Chinese Academy of Sciences key project "The Interannual Variability and Predictability of East Asian Monsoon".

REFERENCES

Gaswami B.N., V. Krishnamurti, and A. Annamalai, 1997: A broad scale circulation index for the interannual variability of the Indian summer monsoon. Report No. 46 (available from the Center for Ocean−Land−Atmosphere Studies (COLA). MD 20705−3136, USA).

Ju J., and J.M. Slingo, 1995: The Asian summer monsoon and ENSO. *Quart. J. Roy. Meteorol. Soc.*, **122**, 1133−1168.

Li C.Y., 1988: Frequent strong activities of East Asian trough and the occurrence of the El Nino event. *Science in China* (series B), 667−674.

National Research Council, 1996: *Learning to predict climate variations associated with El Nino and the Southern Oscillation*. National Academy Press, Washington D.C.

Ropelewski C. F., and M. S. Halpert, 1987: Global and regional scale precipitation patterns associated with the El Nino / Southern Oscillation. *Mon. Wea. Rev.*, **115**, 1606−1626.

Sellers P.J., Y. Mintz, Y.C. Sud, and A. Dalcher, 1986: A simple biosphere model (SiB) for use within general circulation models. *J. Atmos. Sci.*, **43**, 505−531.

Tao S.Y., and L.X. Chen, 1987: A review of recent research on the East Asian monsoon in China. *Monsoon Meteorology*, Oxford University Press, 60−92.

Wang B., and Z. Fan, 1998: On choice of dynamically coherent South Asian summer monsoon indices. *Asian Monsoon and China Heavy Rain*, Edited by Institute of Atmospheric Physics, China Meteorological Press, Beijing, 170−183 (in Chinese).

Webster P.J., and S. Yang, 1992: Monsoon and ENSO: Selectively interactive systems. *Quart. J. Roy. Meteorol. Soc.*, **118**, 877−926.

Wu Guoxiong, Liu Hui, Zhao Yucheng, and Li Weiping, 1996: A nine−layer atmospheric general circulation model. *Advances in Atmospheric Sciences*, **13**, 1−18.

Wu G.X., X.H. Zhang, H. Liu, Y.Q. Yu, X.Z. Jin, Y.F. Guo, S.F. Sun, W.P. Li, B. Wang, and G. Y. Shi, 1997: LASG coupled Ocean Atmosphere−Land model (GOALS / LASG). *J. Appl. Meteorol.*, **8**, 15−28 (in Chinese).

Xue Y. K., P. J. Sellers, J. L. Klinter, and J. Shukla, 1991: A simplified biosphere model for global climate studies. *J. Climate*, **4**, 345−364.

Yu Y. Q., 1997: Coupling scheme of an atmosphere−ocean−sea ice model and the simulation of decadal scale climate variability. PhD thesis, Institute of Atmospheric Physics, Chinese Academy of Sciences, Beijing, 130pp.

Yu Y. Q., 1998: A modified coupling scheme of the ocean−atmosphere flux anomaly (in Chinese). *Chinese Science Bulletin*, **43**, 866−869.

Zhang X.H., K.M. Chen, X.Z. Jin, W.Y. Lin, and Y.Q. Yu, 1996: Simulation of thermalhaline circulation with a twenty−layer oceanic general circulation model. *Theor. Appl. Cli.*, **55(1−4)**, 65−88.

Zeng Q.C., X.H. Zhang, X.Z. Liang, C.G. Yuan, and S.F. Chen, 1989: Documentation of IAP two−level atmospheric general circulation model. DOE / ER / 60314−HI.